JAEA-Research
2007-094

A Study on Extrusion Behavior of Buffer Material into Fractures using X-ray CT Method

Kenji TANAI and Kazuhiro MATSUMOTO*

Near-Field Research Group
Geological Isolation Research and Development Directorate

February 2008

Japan Atomic Energy Agency

日本原子力研究開発機構

JAEA-Research

本レポートは日本原子力研究開発機構が不定期に発行する成果報告書です。
本レポートの入手並びに著作権利用に関するお問い合わせは、下記あてにお問い合わせ下さい。
なお、本レポートの全文は日本原子力研究開発機構ホームページ（http://www.jaea.go.jp/index.shtml）より発信されています。このほか財団法人原子力弘済会資料センター*では実費による複写頒布を行っております。

〒319-1195　茨城県那珂郡東海村白方白根 2 番地 4
日本原子力研究開発機構　研究技術情報部　研究技術情報課
電話 029-282-6387, Fax 029-282-5920

*〒319-1195　茨城県那珂郡東海村白方白根 2 番地 4　日本原子力研究開発機構内

This report is issued irregularly by Japan Atomic Energy Agency
Inquiries about availability and/or copyright of this report should be addressed to
Intellectual Resources Section, Intellectual Resources Department,
Japan Atomic Energy Agency
2-4 Shirakata Shirane, Tokai-mura, Naka-gun, Ibaraki-ken 319-1195 Japan
Tel +81-29-282-6387,　Fax +81-29-282-5920

A Study on Extrusion Behavior of Buffer Material into Fractures using X-ray CT Method

Kenji TANAI and Kazuhiro MATSUMOTO[*1]

Geological Isolation Research Unit
Geological Isolation Research and Development Directorate
Japan Atomic Energy Agency
Tokai-mura, Naka-gun, Ibaraki-ken

(Received December 25, 2007)

The buffer material that will be used as a component of the engineered barriers system for geological disposal of high-level radioactive waste is designed to swell when it becomes saturated by groundwater. As a result of the swelling, bentonite buffer material may penetrate through open fractures into the surrounding host rock. If it is sustained for extremely long periods of time, the bentonite extrusion could lead to reduction of the buffer density, which may in turn degrade the expected performance (e.g. low permeability, diffusion control, colloid filtration, load-bearing capacity, etc). In this study, extrusion test with X-ray CT measurement was carried out to clarify the mechanical behavior of bentonite extrusion through fractures in the surrounding rock. In the extrusion test, the out flow distance into fracture is affected by bentonite content ratio and ionic strength of ground water. X-ray CT measurement is available to evaluate the density distribution of bentonite into the fractures. The X-ray CT measurement will play an important role for study of extrusion behavior of buffer material, particularly for development of extrusion models for compacted bentonite.

Keywords: Bentonite, Extrusion Behavior, X-ray CT Method,

[*1] Inspection Development Corporation

X線CT法を用いた岩盤亀裂中への緩衝材の侵入挙動に関する研究

日本原子力研究開発機構　地層処分研究開発部門
地層処分基盤研究開発ユニット

棚井　憲治，松本　一浩[*1]

(2007年12月25日受理)

高レベル放射性廃棄物の地層処分における人工バリアシステムの一つである緩衝材は，地下水の浸潤により膨潤し，それによって周辺岩盤に存在する開口亀裂に侵入する。仮に亀裂への侵入が長期間にわたり継続される場合には，緩衝材密度の低下を招くことになり，低透水性，核種移行抑制機能およびコロイドろ過性などといった緩衝材に期待されている性能に悪影響を及ぼすことが懸念される。本研究では，岩盤亀裂中への緩衝材の侵入挙動を明らかにするために，X線CT測定を併用した侵入試験を行った。

侵入試験については，亀裂中への侵入距離がベントナイト配合率や地下水のイオン強度に影響されることがわかった。X線 CT 測定に関しては，緩衝材の侵入挙動の把握，特に侵入モデルの開発の観点からも重要な役割を果たすものとなる。

核燃料サイクル工学研究所：〒319-1194　茨城県那珂郡東海村村松4-33
[*1]　検査開発株式会社

Contents

目　　次

1. Introduction

As a candidate buffer material for the engineered barriers system (EBS) of high level radioactive waste geological disposal, compacted bentonite has a number of favorable properties, such as its low permeability and high sorption capacity for radionuclide migration. Furthermore, as the bentonite will be resaturated and swelled gradually after repository closure, not only will any gaps within the bentonite be sealed, but the bentonite may also be excluded into fractures in the surrounding rock, diverting a part of the water flow away from the repository. This situation is potentially advantageous to repository safety. However, if loss of bentonite into fractures due to extrusion and subsequent erosion of the extruding front by groundwater flow is too much increased, then the decrease in density of the bentonite within the buffer may lead to reduce its favorable properties. Therefore, the extrusion and erosion of bentonite buffer from the disposal pit or the disposal tunnel should be quantitatively understood to ensure its long-term EBS performance for the geological disposal. From this point of view, an attempt was made to use X-ray computed tomography (X-ray CT) technique to non-destructively measure the density distribution of bentonite buffer which was extruded into the artificial fractures.

2. Test methodology

2.1 Extrusion experiment

The test apparatus of buffer extrusion experiment is shown in Figure 1. As shown in the figure, the surrounding host rock is made with the parallel transparent acrylic plates which form the artificial fracture, and the disposal pit is formed by the hole in the center position, in which compacted bentonite is fulfilled. Distilled water or synthetic seawater is supplied to the artificial fracture under pressure, defined by a fixed water head. Water infiltration and buffer swelling behaviors can be observed from the top side and the distance of bentonite intrusion from the center is directly measured by photography. The variable aperture of artificial fracture is a range of 0.5 - 1.5 mm.
The experimental conditions are shown in Table 1. The compositions of the synthetic seawater and groundwater sampled from the Horonobe underground research laboratory site are shown in Table 2 and 3 respectively.
Kunigel V1®, which is produced by Kunimine Industries Co. Ltd, was used for bentonite buffer material, which is a mixture of montmorillonite (59.3 %) and quarts sand (30 %). The other minerals are feldspar (6 %) and calcite (4 %).

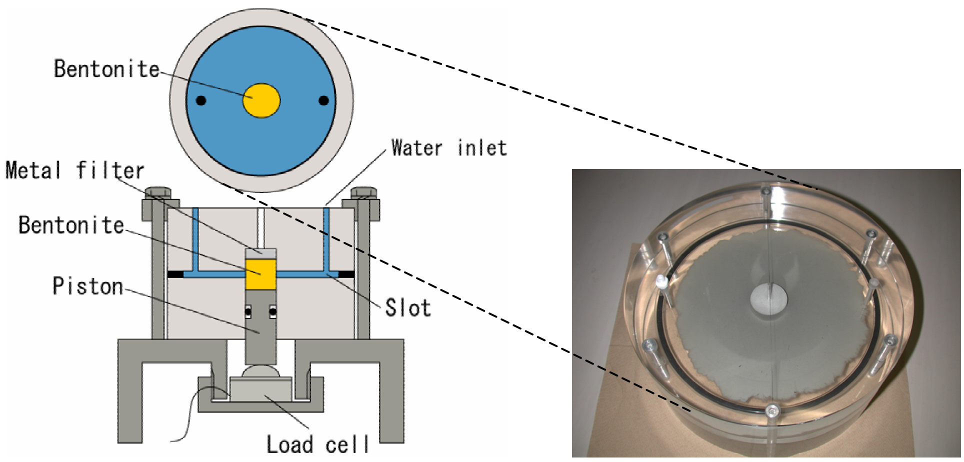

Figure 1 Test apparatus for buffer extrusion experiment

Table 1 Test conditions for extrusion experiment

Test water	Distilled water		Synthetic seawater		Horonobe underground water	
Sand mixtures ratio [%]	0	30	0	30	0	30
Dry density [Mg/m^3]	1.8	1.6, 1.8	1.8	1.6, 1.8	1.8	1.6
Aperture of Fracture [mm]	0.5, 1.0, 1.5					
Bentonite material	Kunigel V1 bentonite					
Sample size [mm]	ϕ 50 x H 50					
Initial water content [%]	7 ~ 10					
Test temperature [ºC]	approximately 20					

Table 2 Composition of synthetic seawater (ASTM D1141-98 standards)

	unit	Analysis results		unit	Analysis results
pH	mS/m	7.93	BO_3^{3-}	ppm	26
EC	ppm		Na^+	ppm	10300
Cl^-	ppm	19200	K^+	ppm	410
SO_4^{2-}	ppm	2740	Ca^{2+}	ppm	420
HCO_3^-	ppm	140	Mg^{2+}	ppm	1310
F^-	ppm	1.2	Sr^{2+}	ppm	61
Br^-	ppm	65	Ionic strength	mol/dm^3	0.64

Table 3 Composition of Horonobe underground water

	unit	Analysis results		unit	Analysis results
pH	-	7.7	Si	mg/ℓ	24
EC	mS/m	2010	Al	mg/ℓ	< 1
Na^+	mg/ℓ	4300	Cl^-	mg/ℓ	6400
K^+	mg/ℓ	92	NO_3^-	mg/ℓ	< 0.1
NH_4^+	mg/ℓ	124	SO_4^{2-}	mg/ℓ	< 0.2
Ca_2^+	mg/ℓ	136	S^{2-}	mg/ℓ	< 0.5
Mg_2^+	mg/ℓ	89	P (alkalinity)	mmol/ℓ	< 0.5
Total P	mg/ℓ	0.45	M (alkalinity)	mmol/ℓ	22.8
I^-	mg/ℓ	19	HCO_3^-	mg/ℓ	1600
Fe^{2+}	mg/ℓ	< 0.2	CO_3^{2-}	mg/ℓ	< 0.5
Fe^{3+}	mg/ℓ	0.6	TOC	mg/ℓ	23
Total Fe	mg/ℓ	0.6	Ionic strength	mol/dm^3	0.2075

2.2 X-ray CT method

The X-ray CT scanner "Asteion VI" (Toshiba Medical Co.) was used for the test. It is a type of the third-generation medical scanner (Figure 2). The response time for image visualization using Fourier transformation is 3.0 seconds. The CT value defined by the degree of X-ray absorption is an output from the X-ray CT scanner, and the CT image is reproduced by a spatial distribution of the digital CT values. The CT value is obtained from the following equation;

$$CT \text{ value} = \frac{\mu - \mu_{\text{water}}}{\mu_{\text{water}}} k \qquad [1]$$

where k is the material constant, μ and μ_{water} are the attenuation coefficients of the material and water, respectively. It is noted that the constant k is here fixed to a value of 1000. Thus, the CT value of air should be -1000 because the coefficient of absorption for air is zero. In general, digital image is composed of units called a "pixel", which shows the image in two dimensions.
The X-ray CT image shows the density distribution in three dimensions and it is composed of units called a "voxel" rather than pixel. The height of the voxel is equal to the attenuation width of the X-ray beam. In addition, the CT image is originally composed of 512 x 512 voxels with 256 levels of black and white colors (Otani et al., 2005). The degree of X-ray attenuation increases linearly with the bulk density of sample.
Figure 3 shows relationship between bulk density and CT value of Kunigel V1 bentonite. It can be noted from Figure 3 that the CT value correlates well with the bulk density of the material. The bulk density of Kunigel V1 bentonite, ρ_b is obtained from the following equation (Tanai and Yamamoto, 2003):

$$\rho_b = \frac{CT + 1465.7}{1495.6} \qquad [2]$$

where "CT" is the CT value of the Kunigel V1 bentonite sample.

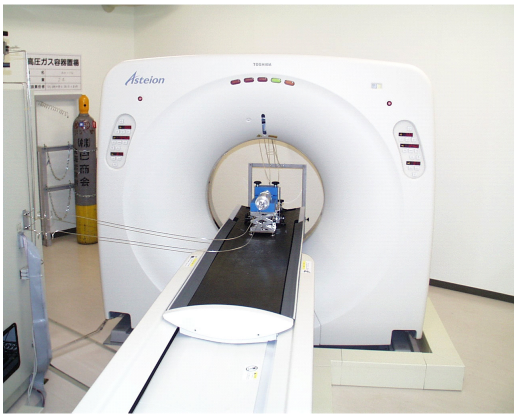

Figure 2 Schematic of the X-ray CT scanner

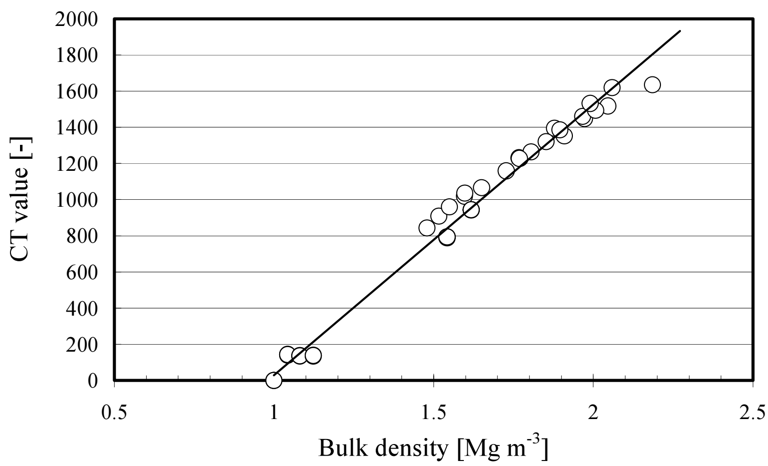

Figure 3 Relationship between the bulk density and CT value of Kunigel V1 bentonite

3. Experimental results

3.1 Extrusion test

Key findings of existing laboratory studies of compacted bentonite extrusion into fractures are that:

- in the absence of erosion, the migration distance is proportional to the square root of time after the contact between water and bentonite, and the extrusion rate is dependent on the fracture width and bentonite content as follows (Kanno & Wakamatsu, 1991; Kanno et al., 1999):

$$y = A(d, Bc)\sqrt{t} \qquad [3]$$

where y is the distance of bentonite outflow in fracture (m), t is the elapsed time (sec), and A is a proportional coefficient depending on the fracture width, d and bentonite content ratio, Bc.

- two regions are detected to develop in the excluding bentonite front: one fairly stiff and very soft (Pusch, 1983),

- the water content in the very soft region just behind the gel front is about 550 %, which is close to the liquid limit of the bentonite clay used (Boisson, 1989)

Figure 4 and 5 show changes with time for the measured outflow distance under the distilled water condition as function of dry densities of Kunigel V1 (1.6 and 1.8 Mg/m^3), sand mixtures ratio (0 % and 30 %) and apertures of artificial fractures (0.5, 1.0 and 1.5 mm) respectively. As the aperture of fracture increases and as the bentonite content increases, the outflow distance tends to increase (Matsumoto and Tanai, 2003a).

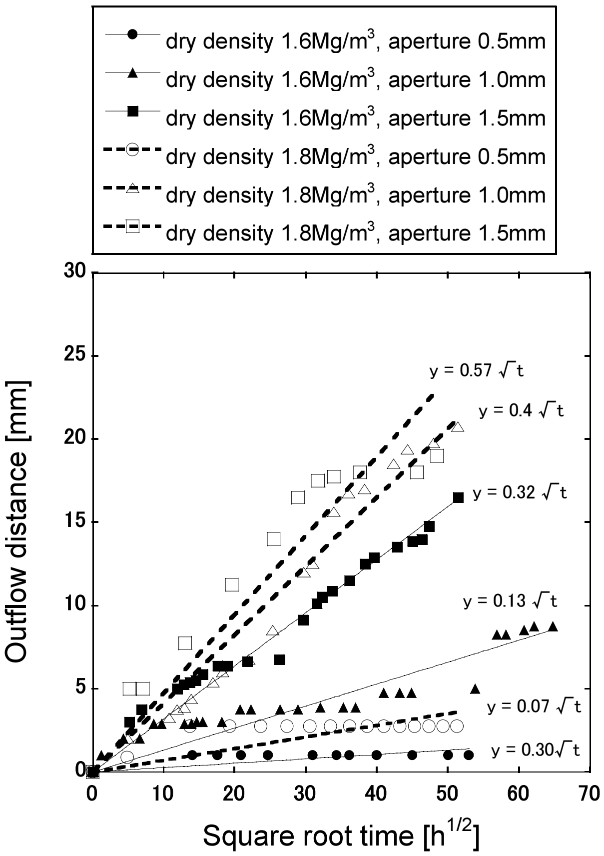

Figure 4 Change of buffer outflow distance with time (sand mixtures ratio 30%)

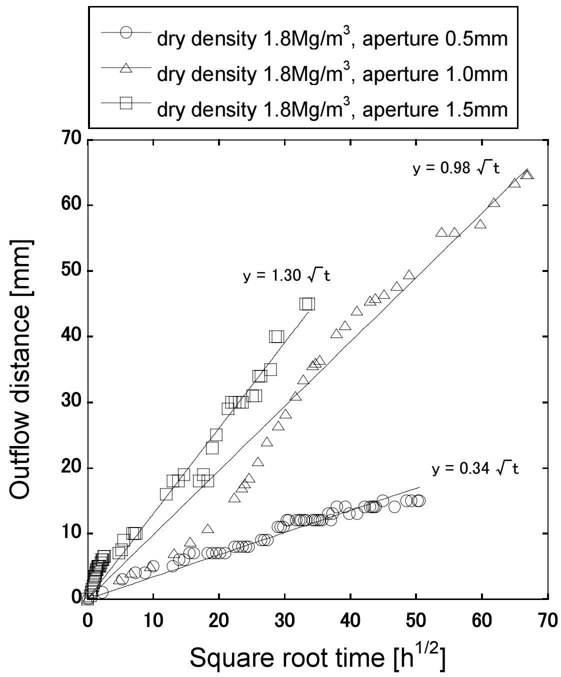

Figure 5 Change of buffer outflow distance with time (sand mixtures ratio 0%)

Figure 6 shows changes with time for the measured outflow distance under the distilled water, Horonobe groundwater and synthetic seawater conditions at a dry density of 1.6 Mg/m^3 (30 wt% sand mixture and aperture of 1.5 mm). The results of bentonite outflow distance at dry density of 1.8 Mg/m^3 (0wt% sand mixture and aperture of 1.5 mm) under the distilled water, the Horonobe groundwater and synthetic seawater conditions are shown in Figure 7 (Matsumoto and Tanai, 2003a, 2003b, 2005). The basic mechanism of the extrusion phenomenon is thought to be free expansion of bentonite particle structure due to its swelling property. The swelling properties of Kunigel V1 bentonite decrease due to the effect of salinity (Kikuchi et al., 2005). Therefore, the bentonite outflow distance into the fracture with synthetic seawater is smaller than that with distilled water.

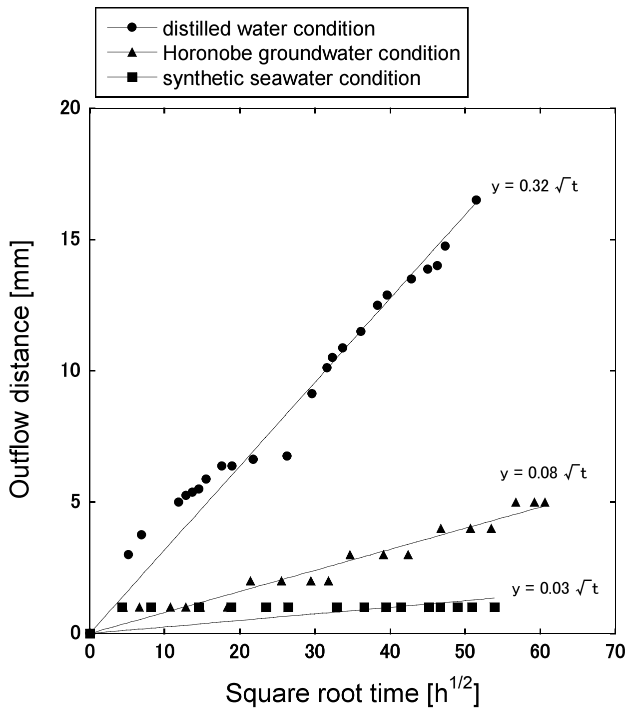

Figure 6 Change of buffer outflow distance with time (dry density of 1.6 Mg/m^3)

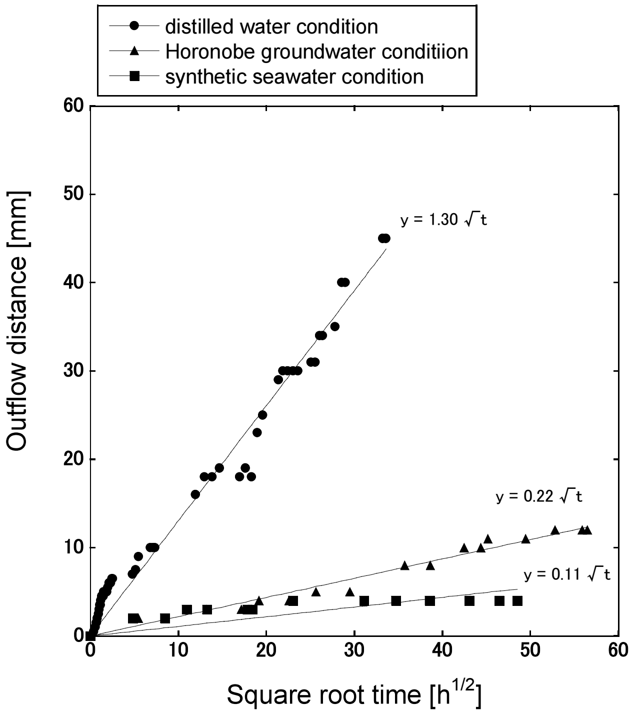

Figure 7 Change of buffer outflow distance with time (dry density of 1.8 Mg/m^3)

Figure 8 shows correlation between effective clay density and proportional coefficient on fracture aperture of 1.5 mm under the distilled water and synthetic seawater conditions. The proportional coefficient “ A ” for each condition is described as follows (Matsumoto and Tanai, 2003b, 2005);

$$A = 3.53 \times 10^{-3} \cdot \exp(3.26\rho_e) \text{ (distilled water condition)} \quad [4]$$

$$A = 5.47 \times 10^{-4} \cdot \exp(3.01\rho_e) \text{ (synthetic seawater condition)} \quad [5]$$

where ρ_e is effective clay density (Mg/m^3).

Figure 9 shows correlation between ionic strength and proportional coefficient on fracture aperture of 1.5mm. The out flow distance into fracture is affected by ionic strength of groundwater.

The effective clay density (index obtained from calculation of the dry density of the bentonite excluding the sand volume) is given by the following equation;

$$\rho_e = \frac{M_b}{(V_b + V_a)} = \frac{\rho_d(100 - R_s)}{\left(100 - \frac{\rho_d R_s}{\rho_s}\right)} \quad [6]$$

where ρ_e is effective clay density (Mg/m^3); M_b is the dry weight of bentonite (Mg); V_b is the volume of bentonite (m^3); V_a is the volume of void (m^3); ρ_d is the dry density of bentonite/sand mixture (Mg/m^3); R_s is the mixing ratio at dry weight of sand (wt%); ρ_s is the density of soil particle of sand (Mg/m^3).

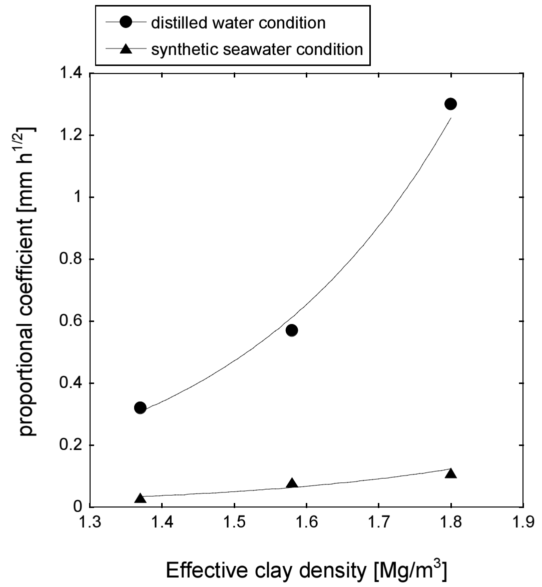

Figure 8 Relationship between effective clay density and proportional coefficient

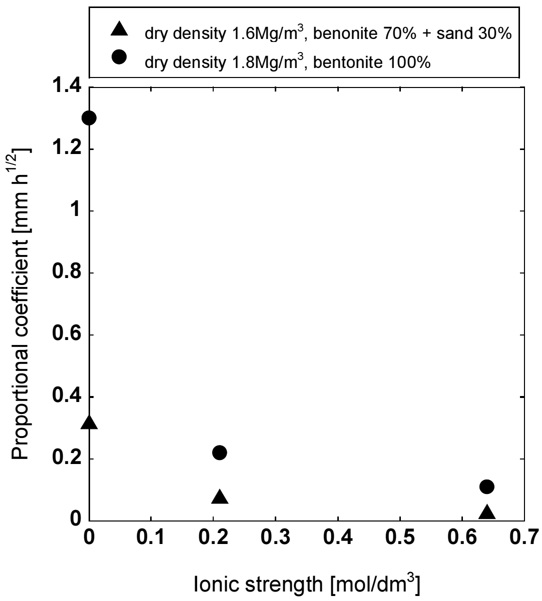

Figure 9 Relationship between ionic strength and proportional coefficient

3.2 X-ray CT measurement

<u>Application of X-ray CT method</u>

This was carried out to clarify the issues for application of X-ray CT measurement of density distribution of bentonite within the fracture. The test equipment is shown in Figure 10. The distilled water was supplied to the water inlet port, and the bentonite material was excluded into the plastic pipe as a result of its swelling. The measurement procedure of density distribution in the plastic pipe was as follows; i) measurement of the X-ray CT with scanning thickness of 1.0mm (Figure 11 and Table 4) and then calculation of bulk density using the CT value and equation [2]; ii) removal of the plastic pipe from the test equipment after X-ray CT measurement, and then cutting it into about 12 pieces; iii) water content measurement for each piece by oven-drying and then calculation of density distribution in the plastic pipe. The relationship between outflow distance and bulk density of bentontie in the plastic pipe is shown in Figure 12 (Matsumoto and Tanai, 2003b). The CT measurement indicates a similar tendency with the oven-drying method. Thus, the X-ray CT method is applicable to evaluate the density distribution of bentonite extruded into the fractures in a non-destructive manner.

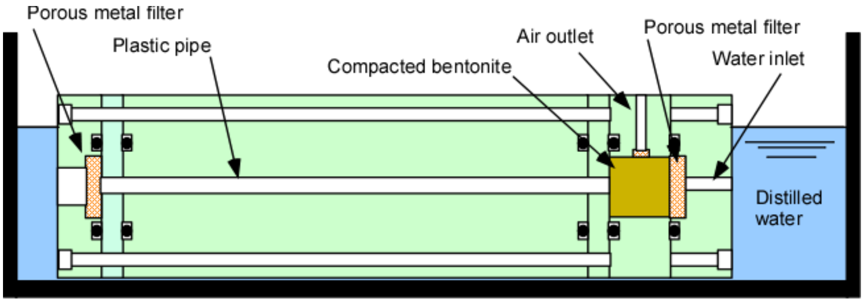

Figure 10 Concept of applicability test

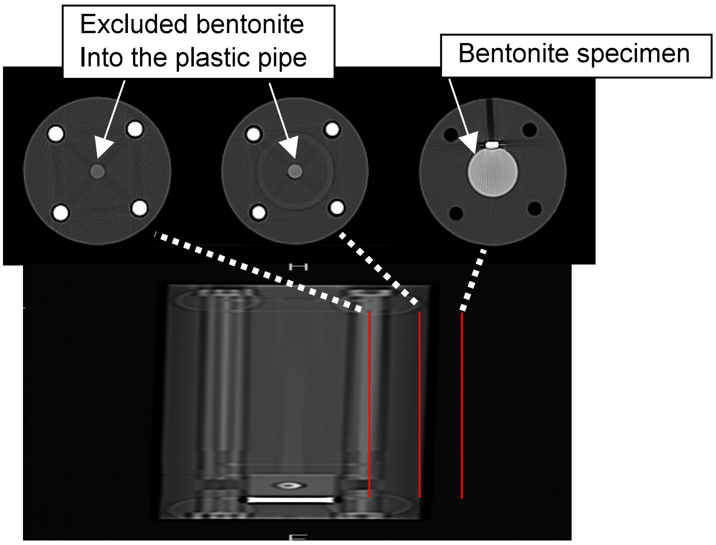

Figure 11 Scanning image

Table 4 Condition of applicability test

Specimen size [mm]	ϕ 20 x H 20	Diameter of plastic pipe [mm]	6.0
Dry density [Mg/m3]	1.6	Experimental solution	Distilled water
Sand mixture ratio [%]	0.0	Experimental periods [day]	77.0
Initial water content [%]	11.0	Temperature [ºC]	20.0

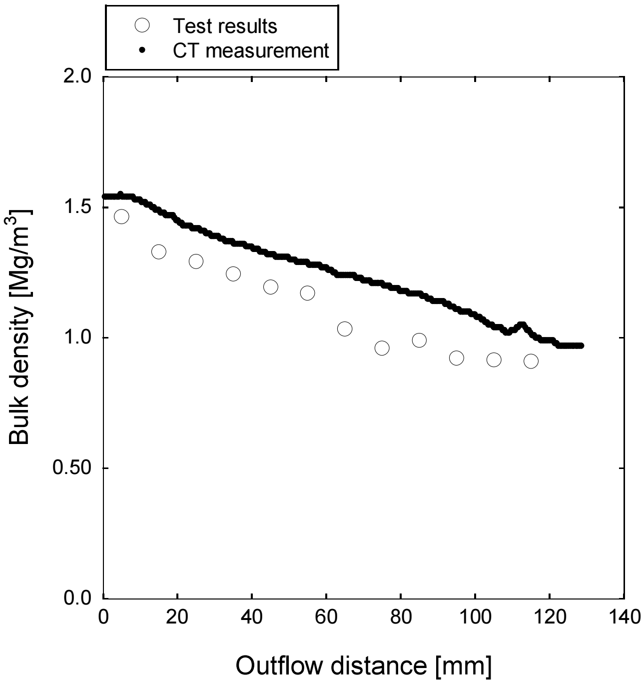

Figure 12 Comparison of CT measurement and oven-drying method

Application of X-ray CT method for the extrusion experiment

The X-ray CT method is applicable to evaluate the density distribution of bentonite extruded into the fractures. Therefore, this was carried out to obtain the density distribution of bentonite into the fractures for extrusion experiment. The X-ray CT measurement conditions and scanning position in this test are shown in Table 5 and Figure 13 respectively. The density distribution of bentonite in the fracture is measured at the same measurement position as function of time. The relationship between the outflow distance and bulk density of bentontie extruded into the fractures as function of time is shown in Figure 14 (Matsumoto and Tanai, 2005).

The X-ray CT method is found available to evaluate the density distribution in a non-distractive manner and demonstrated as a powerful experimental tool. Since it is inevitable that the X-ray CT image involves high noise content, the denoising is essential for the analysis. Among them, the stacking technique is commonly used and effective to reduce by imposing plural images taken at the same position under the same conditions (Sato et al., 2003). In this study, the tomography images were taken for 30 times at the same cross section under the same conditions.

Table 5 X-ray CT measurement conditions

voltage	135 kV
Current	150 mA
Slice thickness	1 mm
Scan time	1.0 sec
Scan position	One cross section (Figure 13)

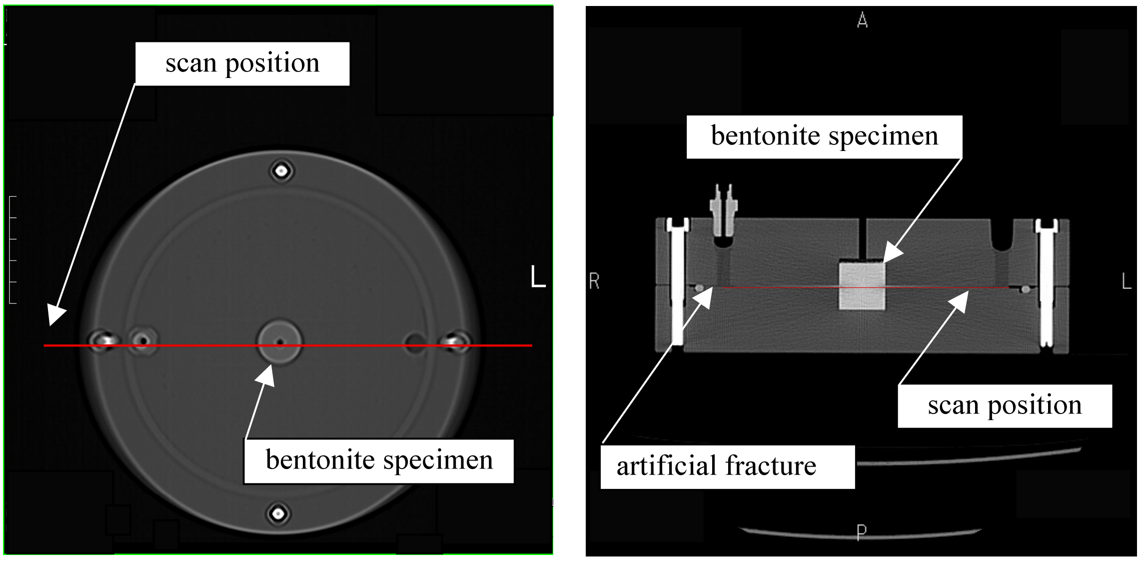

Figure 13 scan position of X-ray CT measurement

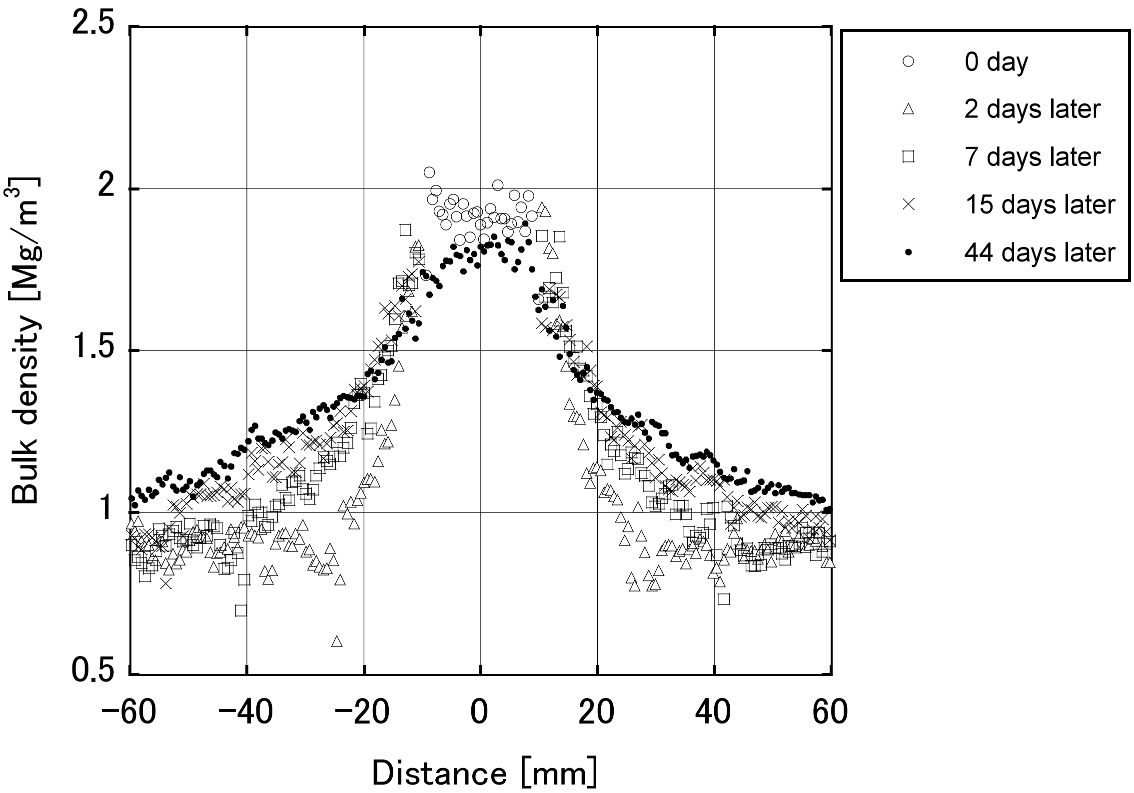

Figure 14 Relationship between outflow distance and density distribution into fracture with time

4. Conclusions

The extrusion experiment of bentonite buffer material was carried out to clarify the mechanical behavior of bentontie extruded into fractures, which was anticipated to depend on parameters of sand mixtures ratio, aperture of fracture and so on. It was found that the outflow distance in fractures was affected by bentonite content ratio and ionic strength of groundwater. The proportional coefficient “A” under the distilled water and synthetic seawater conditions were also obtained from the experiment.

It was concluded that X-ray CT was useful for characterization of the extrusion properties of bentonite, in terms of evaluation of the density distribution in a non-distractive manner. The X-ray CT method will play an important role for study of the extrusion behavior of buffer material, particularly for development of the extrusion models. It is expected that these understanding of the mechanism would be further improved by studies using more higher resolution X-ray CT.

References

Boisson, J.Y. (1989): Study on the possibilities by flowing ground waters on bentonite plugs expanded from borehole into fractures, Proc. NEA/CEC Workshop – Sealing of Radioactive Waste Repositories.

Kanno, T. and Wakamatsu, H. (1991): Experimental study on bentonite gel migration from a deposition hole, Proc. 3rd Int. Conf. Nuclear Fuel Reprocessing and Waste Management (RECOD ’91).

Kanno, T., Matsumoto, K. and Sugino, H. (1999): Evaluation of extrusion and erosion of bentonite buffer, Proc. 7th Int. Conf. on Radioactive Waste Management and Environmental Remediation (ICEM ’99).

Kikuchi, H., Tanai, K. and Yui, M. (2005): Database development of fundamental properties for the buffer material in Japan, GLOBAL 2005, Paper No.238.

Matsumoto, K. and Tanai, K. (2003a): Evaluation of the outflow characteristic of bentonite buffer material (II), Research document, JNC TN8400 2003-006 (in Japanese).

Mastumoto, K. and Tanai, K. (2003b): Extrusion and erosion of bentonite buffer, Research document, JNC TN8400 2003-035 (in Japanese).

Matsumoto, K. and Tanai, K. (2005): Extrusion and erosion of bentonite buffer (II), JNC Technical Report, JNC TN8400 2004-026 (in Japanese).

Otani, J., Mukunoki, T. and Sugawara, K. (2005): Evaluation of particle crushing in soils using X-ray CT data, Soils and Foundations vol 45, No.1, pp. 99-108.

Pusch, R. (1983): Stability of bentonite gels in crystalline rock – Physical Aspects. SKBF/SKB Technical Report 83-04.

Sato, A., Fukahori. D. and Sugawara. K. (2003): Crack opening analysis by the X-ray CT image subtraction method, International Workshop on X-ray CT for Geomaterials, GEOX 2003, pp.223-228.

Tanai, K. and Yamamoto, M. (2003): Experimental and modeling studies on gas migration in Kunigel V1 bentonite, Research document, JNC TN8400 2003-024.

国際単位系（SI）

表１．SI 基本単位

基本量	SI 基本単位	
	名称	記号
長さ	メートル	m
質量	キログラム	kg
時間	秒	s
電流	アンペア	A
熱力学温度	ケルビン	K
物質量	モル	mol
光度	カンデラ	cd

表２．基本単位を用いて表されるSI組立単位の例

組立量	SI 基本単位	
	名称	記号
面積	平方メートル	m^2
体積	立法メートル	m^3
速さ，速度	メートル毎秒	m/s
加速度	メートル毎秒毎秒	m/s^2
波数	毎メートル	m-1
密度（質量密度）	キログラム毎立法メートル	kg/m^3
質量体積（比体積）	立法メートル毎キログラム	m^3/kg
電流密度	アンペア毎平方メートル	A/m^2
磁界の強さ	アンペア毎メートル	A/m
（物質量の）濃度	モル毎立方メートル	mol/m^3
輝度	カンデラ毎平方メートル	cd/m^2
屈折率	（数の）１	1

表５．SI 接頭語

乗数	接頭語	記号	乗数	接頭語	記号
10^{24}	ヨタ	Y	10^{-1}	デシ	d
10^{21}	ゼタ	Z	10^{-2}	センチ	c
10^{18}	エクサ	E	10^{-3}	ミリ	m
10^{15}	ペタ	P	10^{-6}	マイクロ	µ
10^{12}	テラ	T	10^{-9}	ナノ	n
10^{9}	ギガ	G	10^{-12}	ピコ	p
10^{6}	メガ	M	10^{-15}	フェムト	f
10^{3}	キロ	k	10^{-18}	アト	a
10^{2}	ヘクト	h	10^{-21}	ゼプト	z
10^{1}	デカ	da	10^{-24}	ヨクト	y

表３．固有の名称とその独自の記号で表されるSI組立単位

組立量	SI 組立単位			
	名称	記号	他のSI単位による表し方	SI基本単位による表し方
平面角	ラジアン[a]	rad		$m\cdot m^{-1}=1$[b]
立体角	ステラジアン[a]	sr[c]		$m^2\cdot m^{-2}=1$[b]
周波数	ヘルツ	Hz		s^{-1}
力	ニュートン	N		$m\cdot kg\cdot s^{-2}$
圧力，応力	パスカル	Pa	N/m^2	$m^{-1}\cdot kg\cdot s^{-2}$
エネルギー，仕事，熱量	ジュール	J	N・m	$m^2\cdot kg\cdot s^{-2}$
工率，放射束	ワット	W	J/s	$m^2\cdot kg\cdot s^{-3}$
電荷，電気量	クーロン	C		s・A
電位差（電圧），起電力	ボルト	V	W/A	$m^2\cdot kg\cdot s^{-3}\cdot A^{-1}$
静電容量	ファラド	F	C/V	$m^{-2}\cdot kg^{-1}\cdot s^4\cdot A^2$
電気抵抗	オーム	Ω	V/A	$m^2\cdot kg\cdot s^{-3}\cdot A^{-2}$
コンダクタンス	ジーメンス	S	A/V	$m^{-2}\cdot kg^{-1}\cdot s^3\cdot A^2$
磁束	ウエーバ	Wb	V・s	$m^2\cdot kg\cdot s^{-2}\cdot A^{-1}$
磁束密度	テスラ	T	Wb/m^2	$kg\cdot s^{-2}\cdot A^{-1}$
インダクタンス	ヘンリー	H	Wb/A	$m^2\cdot kg\cdot s^{-2}\cdot A^{-2}$
セルシウス温度	セルシウス度[d]	℃		K
光束	ルーメン	lm	cd・sr[c]	$m^2\cdot m^{-2}\cdot cd=cd$
照度	ルクス	lx	lm/m^2	$m^2\cdot m^{-4}\cdot cd=m^{-2}\cdot cd$
（放射性核種の）放射能	ベクレル	Bq		s^{-1}
吸収線量，質量エネルギー分与，カーマ	グレイ	Gy	J/kg	$m^2\cdot s^{-2}$
線量当量，周辺線量当量，方向性線量当量，個人線量当量，組織線量当	シーベルト	Sv	J/kg	$m^2\cdot s^{-2}$

(a) ラジアン及びステラジアンの使用は、同じ次元であっても異なった性質をもった量を区別するときの組立単位の表し方として利点がある。組立単位を形作るときのいくつかの用例は表４に示されている。
(b) 実際には、使用する時には記号rad及びsrが用いられるが、習慣として組立単位としての記号“１”は明示されない。
(c) 測光学では、ステラジアンの名称と記号srを単位の表し方の中にそのまま維持している。
(d) この単位は、例としてミリセルシウス度m℃のようにSI接頭語を伴って用いても良い。

表４．単位の中に固有の名称とその独自の記号を含むSI組立単位の例

組立量	SI 組立単位		
	名称	記号	SI 基本単位による表し方
粘度	パスカル秒	Pa・s	$m^{-1}\cdot kg\cdot s^{-1}$
力のモーメント	ニュートンメートル	N・m	$m^2\cdot kg\cdot s^{-2}$
表面張力	ニュートン毎メートル	N/m	$kg\cdot s^{-2}$
角速度	ラジアン毎秒	rad/s	$m\cdot m^{-1}\cdot s^{-1}=s^{-1}$
角加速度	ラジアン毎平方秒	rad/s^2	$m\cdot m^{-1}\cdot s^{-2}=s^{-2}$
熱流密度，放射照度	ワット毎平方メートル	W/m^2	$kg\cdot s^{-3}$
熱容量，エントロピー	ジュール毎ケルビン	J/K	$m^2\cdot kg\cdot s^{-2}\cdot K^{-1}$
質量熱容量（比熱容量），質量エントロピー	ジュール毎キログラム毎ケルビン	J/(kg・K)	$m^2\cdot s^{-2}\cdot K^{-1}$
質量エネルギー（比エネルギー）	ジュール毎キログラム	J/kg	$m^2\cdot s^{-2}\cdot K^{-1}$
熱伝導率	ワット毎メートル毎ケルビン	W/(m・K)	$m\cdot kg\cdot s^{-3}\cdot K^{-1}$
体積エネルギー	ジュール毎立方メートル	J/m^3	$m^{-1}\cdot kg\cdot s^{-2}$
電界の強さ	ボルト毎メートル	V/m	$m\cdot kg\cdot s^{-3}\cdot A^{-1}$
体積電荷	クーロン毎立方メートル	C/m^3	$m^{-3}\cdot s\cdot A$
電気変位	クーロン毎平方メートル	C/m^2	$m^{-2}\cdot s\cdot A$
誘電率	ファラド毎メートル	F/m	$m^{-3}\cdot kg^{-1}\cdot s^4\cdot A^2$
透磁率	ヘンリー毎メートル	H/m	$m\cdot kg\cdot s^{-2}\cdot A^{-2}$
モルエネルギー	ジュール毎モル	J/mol	$m^2\cdot kg\cdot s^{-2}\cdot mol^{-1}$
モルエントロピー，モル熱容量	ジュール毎モル毎ケルビン	J/(mol・K)	$m^2\cdot kg\cdot s^{-2}\cdot K^{-1}\cdot mol^{-1}$
照射線量（Ｘ線及びγ線）	クーロン毎キログラム	C/kg	$kg^{-1}\cdot s\cdot A$
吸収線量率	グレイ毎秒	Gy/s	$m^2\cdot s^{-3}$
放射強度	ワット毎ステラジアン	W/sr	$m^4\cdot m^{-2}\cdot kg\cdot s^{-3}=m^2\cdot kg\cdot s^{-3}$
放射輝度	ワット毎平方メートル毎ステラジアン	$W/(m^2\cdot sr)$	$m^2\cdot m^{-2}\cdot kg\cdot s^{-3}=kg\cdot s^{-3}$

表６．国際単位系と併用されるが国際単位系に属さない単位

名称	記号	SI 単位による値
分	min	1 min=60s
時	h	1h =60 min=3600 s
日	d	1 d=24 h=86400 s
度	°	1° =(π/180) rad
分	’	1’ =(1/60)° =(π/10800) rad
秒	”	1” =(1/60)’ =(π/648000) rad
リットル	l、L	$1l=1\ dm^3=10^{-3}m^3$
トン	t	$1t=10^3$ kg
ネーパ	Np	1Np=1
ベル	B	1B=(1/2)ln10(Np)

表７．国際単位系と併用されこれに属さない単位で
SI単位で表される数値が実験的に得られるもの

名称	記号	SI 単位であらわされる数値
電子ボルト	eV	$1eV=1.60217733(49)\times10^{-19}J$
統一原子質量単位	u	$1u=1.6605402(10)\times10^{-27}kg$
天文単位	ua	$1ua=1.49597870691(30)\times10^{11}m$

表８．国際単位系に属さないが国際単位系と
併用されるその他の単位

名称	記号	SI 単位であらわされる数値
海里		１海里=1852m
ノット		１ノット=１海里毎時=(1852/3600)m/s
アール	a	$1\ a=1\ dam^2=10^2m^2$
ヘクタール	ha	$1\ ha=1\ hm^2=10^4m^2$
バール	bar	$1\ bar=0.1MPa=100kPa=1000hPa=10^5Pa$
オングストローム	Å	$1\ Å=0.1nm=10^{-10}m$
バーン	b	$1\ b=100fm^2=10^{-28}m^2$

表９．固有の名称を含むCGS組立単位

名称	記号	SI 単位であらわされる数値
エルグ	erg	$1\ erg=10^{-7}\ J$
ダイン	dyn	$1\ dyn=10^{-5}N$
ポアズ	P	$1\ P=1\ dyn\cdot s/cm^2=0.1Pa\cdot s$
ストークス	St	$1\ St =1cm^2/s=10^{-4}m^2/s$
ガウス	G	$1\ G\ \hat{}\ 10^{-4}T$
エルステッド	Oe	$1\ Oe\ \hat{}\ (1000/4\pi)A/m$
マクスウェル	Mx	$1\ Mx\ \hat{}\ 10^{-8}Wb$
スチルブ	sb	$1\ sb =1cd/cm^2=10^4cd/m^2$
ホト	ph	$1\ ph=10^4lx$
ガル	Gal	$1\ Gal =1cm/s^2=10^{-2}m/s^2$

表10．国際単位に属さないその他の単位の例

名称	記号	SI 単位であらわされる数値
キュリー	Ci	$1\ Ci=3.7\times10^{10}Bq$
レントゲン	R	$1\ R = 2.58\times10^{-4}C/kg$
ラド	rad	$1\ rad=1cGy=10^{-2}Gy$
レム	rem	$1\ rem=1\ cSv=10^{-2}Sv$
X線単位		$1X\ unit=1.002\times10^{-4}nm$
ガンマ	γ	$1\gamma=1\ nT=10^{-9}T$
ジャンスキー	Jy	$1\ Jy=10^{-26}W\cdot m^{-2}\cdot Hz^{-1}$
フェルミ		$1\ fermi=1\ fm=10^{-15}m$
メートル系カラット		$1\ metric\ carat = 200\ mg = 2\times10^{-4}kg$
トル	Torr	1 Torr = (101 325/760) Pa
標準大気圧	atm	1 atm = 101 325 Pa
カロリー	cal	
ミクロン	µ	$1\ \mu=1\mu m=10^{-6}m$

（第７版，1998年改訂）